The thing with the Golgi apparatus

Gert-Jan Both

Supervised by:

P. Sens

C. Storm

Technical university of Eindhoven

January-November 2018

Abstract

Lorem ipsum dolor sit amet, consectetur adipiscing elit. Nam et turpis gravida, lacinia ante sit amet, sollicitudin erat. Aliquam efficitur vehicula leo sed condimentum. Phasellus lobortis eros vitae rutrum egestas. Vestibulum ante ipsum primis in faucibus orci luctus et ultrices posuere cubilia Curae; Donec at urna imperdiet, vulputate orci eu, sollicitudin leo. Donec nec dui sagittis, malesuada erat eget, vulputate tellus. Nam ullamcorper efficitur iaculis. Mauris eu vehicula nibh. In lectus turpis, tempor at felis a, egestas fermentum massa.

Contents

1

Introduction

2

Introduction

3

Data processing pipeline

In this chapter I present the work done on processing the rush movies. Several preprocssing steps hav been undertaken to improve the quality of the fit, and we present all here. Roughly, we can divide the process in four steps:

1. Segmentation and creation of masks
2. Denoising of movies
3. Calculation of spatial and temporal derivatives
4. The actual fitting

Below we describe each step separately.

3.1 STEP 1: SEGMENTATION

The images obtained from the rush experiments often contain multiple cells. Furthermore, we can also segment the image into roughly three different types: 1) the background, where nothing of interest happens. No cells are present here, 2) the cytoplasm, which is the area where we want to fit our model and 3) the Golgi itself, where we do not necessarily want to fit. Unfortunately, no bright field images were available, making segmentation significantly harder, as no clear cell boundary can be observed. Further complicating the story is the large dynamic range of the movies due to the fluorescence concentrating in the Golgi. The following procedures we present have been developed to deal with these problems. Note that they are empirical methods, i.e. there's no theoretical background as to why they *should* work. However, in practice they do and I haven't found any other method which was able to.

3.1.1 VORONOI DIAGRAM

This method is based on a technique called Voronoi tesselation and doesn't depend on ny measure of the intensity. It was developed after noting that since the cargo is spread throughout the ER in the first few frames and as the ER is roughly circumnuclear, we can use this to determine the centre of the cell (roughly). Voronoi tesselation then allows us to divide the frame into areas with just one point per area, i.e. one cell per area (theoretically). More precise, given n coordinates, voronoi tesselation divides the given area into n pieces, where every point in a piece is closest to one coordinate. In practice this means for us that each point in a cell area is closest to its the given cell centre. Figure **ref** shows this. Each calculated cell centre is a red point and the lines depict the borders between each voronoi cell. Assuming the cells don't move too much, they don't cross the cells and thus we apply the voronoi diagram calculated in the first few frames to the entire movie.

3.1.2 Intensity

For the fitting however we wish to make a slightly better approach than a voronoi diagram. As stated, we can't find the exact delineation of the cell, but looking at the intensity, we can see an 'area' of interest, separating background from the cell. Since the Golgi is quite bright in het last 200 or so frames, we consider only the intensity for the Golgi, while for the cytoplasm we consider both the intensity and its time derivative. Thus we have two analog but different processes. For the Golgi we do the following:

1. Renormalize the concentration C between 0 and 1.
2. Sum all frames. One then obtains an image such as figure **ref**

$$x \sum_{frames} C(x, y, t)$$

3. This image is thresholded, either through an otsu threshold or a manual one, until the mask roughly matches what we want. Note that extreme precision isn't required, since we just want the rough area. THis results in figure **ref**

For the cytoplasm we follow the same procedure only now we take the log of sum of the product of the intensity and its time derivative:

$$\log \left(\sum_{frames} C(x, y, t) \cdot \partial_t C(x, y, t) \right)$$

We thus obtain a complete mask for the movie as shown in figure **ref**

3.2 Step 2 - Denoising

In order to accurately calculate the derivatives and generally improve the quality of fitting, we wish to denoise and smooth the obtained movies. Denoising and

smoothing is a subject about which many books have been written and there are hundreds of approaches. One oft-used technique is to Fourier transform the signal, cutoff all coefficients above a cutoff frequency and retransform back into the real domain. Next, a Savitzky-Golay filter can be used to finally smooth the result. However, a big issue with all these methods is their non locality. Since our movies have different scales, this is a big problem. Furthermore, they often smooth out sharp peaks. After evaluating several methods, I have settled on a relatively new method presented in **ref**.

The so-called WavinPOD method combines two well-known filtering techniques, known as wavelet filtering and Proper Orthogonal Decomposition. Below we explain each separately. Our explanation is adapted from **ref** and **ref**.

Wavelet filter

A wavelet filter is not really the appropriate name, as its more of a transform.

More about wavelet transform

Proper orthogonal decomposition

Proper orthogonal decomposition is a technique similar to what is known as Principal component Analysis in statistics and falls into the general category of model reduction techniques. It's often used in flow problems to extract coherent structures from turbulent flows. Simply put, in POD we wish to express data as a sum of orthogonal functions, where the basis is determined from the data, i.e. we don't impose something as a fourier basis, etc..

$$f(x, t) = \sum_k g(x)h(t)$$

Basically we're trying to find the eigenfunctions of the data. Full explanation in paper **ref** Each eigenfunction comes with a eigenvalue, which can be interpreted

as the energy of a mode. The higher the eigenvalue, the more important the mode is to the entire signal. To reduce the dimension of the data, we pick a cutoff k_{max} and only use the modes $k < k_{max}$. Several methods are used to determine the cutoff, but often used is the knee-technique. When we plot the log10 spectrum in figure **ref**, one can often observe a 'knee'. Usually this point is taken as the cutoff.

WAVINPOD

WavinPOD combines these two techniques in the following way. First, we decompose our problem with a POD transformation. This yields a set of temporal and spatial modes. We select the most energetic modes and wavelet filter these, before transforming them back to the real domain. As shown in **ref**, combining these techniques has an advantage over others.

In our case, we select the number of modes to be used by hand (30 in the case of MANII) and apply a 3-level db4 wavelet. We use a slightly higher than necessary level to increase smoothness. In the figure below we show the result for both a pixel in time and one time snapshot. Note that the result is significantly smoother, but that smaller details have been preserved.

3.3   STEP 3 - DERIVATIVES

Taking spatial and temporal derivatives of these images is not an entirely trivial operation due to the discreteness of the system. More specifically, taking numerical derivatives of data is extremely hard to do properly and becomes even harder in the presence of noise. Next to basic finite difference methods, one can for example use a linear-least-squares fitted polynomial, smoothing spline or a so-called tikhonov-regularizer **ref needed**. Each method comes with its strengths and weaknesses, but one particularly nasty thing for our context is that they don't scale well to higher dimensions and quickly become computationally expensive.

Another issue related to discretization is the size of the grid w.r.t. the size of the features. To see this, we plot a 2D-gaussian with $\sigma = 1$ in figure **ref**.

As expected, the derivative is normal to the isolines of the object. Now consider the discretized version of the object. Taking the naive spatial derivate w.r.t. to each direction means only considering a single row or column of and taking the derivative in that direction. Figure **ref** shows the result of this operation. An artifact is clearly visible: instead of a nice uniform derivative, we see a 'cross'. This effect is a cause of the discretization grid being too large for some smaller, often bright, objects.

To remedy this, one can for example artificially upscale the grid, interpolate the values inbetween, and take the derivates from this grid. This is not ideal however, since the upscaling requires a large amount of memory and is computationally expensive. Another solution which is common in image processing is applying a *kernel operator*. The advantage of a kernel operator is that it is extremely computationally cheap, as it involves convolving the original picture with a differentiation kernel. The differentiation kernel is an approximate version of a finite difference scheme. We use and show here the Sobel filter, which is the most commonly used one.

In a simple finite central difference scheme, we set

$$\frac{dx}{dt} \approx \frac{x_{i+1} - x_{i-1}}{2h}$$

where h is the distance between two points. In terms of a kernel operator, this would look like (the h drops out as the distance in terms of pixels is 1):

$$\frac{1}{2} \cdot \begin{bmatrix} 1 & 0 & -1 \end{bmatrix}$$

And applying it by convoluting it to a matrix gives the x-derivative:

$$\partial_x A \approx A * \begin{bmatrix} 1 & 0 & -1 \end{bmatrix}$$

and analogous for the y-direction. However, as we've seen, looking at just a single row introduces cross-like artifacts. To remedy this, we wish to include diagonal pixels as well. However, the distance between the diagonal pixels and the center pixel is not 1 but $\sqrt{2}$ and furthermore we need to decompose is it into $\hat{x}$ and $\hat{y}$, introducing another factor $\sqrt{2}$. Thus, one obtains the classis 3×3 Sobel filter **ref**:

$$\mathbf{G}_x = \frac{1}{8} \cdot \begin{bmatrix} 1 & 0 & -1 \\ 2 & 0 & -2 \\ 1 & 0 & -1 \end{bmatrix} \quad \mathbf{G}_y = \frac{1}{8} \cdot \begin{bmatrix} 1 & 2 & 1 \\ 0 & 0 & 0 \\ -1 & -2 & -1 \end{bmatrix}$$

Although not extremely accurate, the Sobel filter seems to do the tricks for us. Several other versions such as Scharr or Prewitt exist, offering several benefits such as rotational symmetry, but we have not pursued these. They just change the coefficients. Although we have shown a 3×3 filter here, the filter can take into account higher order schemes such as a 5×5 or 7×7. The major benefit of the spatial derivatives as a convolution operator is its computational efficiency: convolutional operations are performed parallel and are extremely fast.

For the time derivative, we apply a second order accurate central derivative scheme, while for the spatial derivatives (both first and second order) we apply the 5×5 Sobel filter. We analyze these in the next chapter .

3.4   STEP 4 - FITTING

Now that we have gathered all our data we can use it to fit. We construct a model (advection-diffusion) and then use a 'simple' least-squares fit to obtain an estimate of the diffusion and advection coefficients. We note two extra issues. First, a diffusion coefficient defined positive, i.e. a negative diffusion coefficient is unphysical. We thus make two different fits in the next chapter as a check: one with unconstrained variables, and one where we force $D > 0$.

Secondly, it's highly plausible that the diffusion coefficient and advection are

position and time dependent. One could construct the full model for this and obtain both the coefficients and their derivatives, but its highly unlikely that this will lead to consistent results and it would still need to happen locally. We thus perform a 'moving-window-fit', where we set the width of the time and position window around a central pixel and assume that the diffusion and velocity are smooth and constant enough in that window to ensure a decent fit. In this, it's quite similar to a technique known in computer vision as optical flow.

4

Results data analysis

Here we present the results from our analysis on the RUSH experiments. We only show the results of MANII because this is the only thing we studied.

5

Physics Informed Neural Networks

In the previous chapters we showed the difficulties in fitting a model in the form of a partial differential equation to spatio-temporal data. The method we developed was a classical numerical approach, separating the problem into several substeps such as denoising, smoothing and numerical differentiating. In the last few years machine learning has been slowly making its way into physics. Very recently, a technique generally referred to as Physics Informed Neural Networks (PINNs) have shown great promise as both tools for simulation and model fitting (1, 2, 3, 4, 5). In this chapter, I will evaluate the use of this technique to fit the model to the RUSH data. I've divided the chapter into three parts:

- **Neural Networks** - This part will cover the basics of neural networks: their inner workings, how to train them and other general features.

- **Physics Informed Neural networks** - In this second part we introduce the concept behind PINNs, use it to solve a toy problem and apply it to our RUSH data.
- **Conclusion** - Finally we summarize the results and observations from the previous sections.

5.1 NEURAL NETWORKS

Artificial Neural Networks (ANNs) are networks inspired by biological neural networks. Contrary to other ways of computing, ANNs are not specifically programmed for a task - instead, ANNs are *trained* using a set of data. Research on artificial neural networks started in the '40s but never gained any critical mass, as no efficient training algorithm was known. Once an efficient training algorithm was found in 1975 by Werbos, interest resurged but it wasn't until the late '00s that deep learning started gaining widespread traction. The use of GPU's allowed ANNs to be efficiently trained and widely deployed at reasonable cost.

The advancements in machine learning in general and especially neural networks in the last ten years have yielded a wealth of techniques and approaches. In supervised learning, the network is given pre-labeled data so that it is trained by learning the mapping from the given inputs to the given outputs. Other types such as supervised learning, where the network needs to learns to discriminate between unlabeled data, and reinforcement learning don't have any obvious use for PINNs yet and I've thus chosen to omit them. In the next sections, I'll present the mathematics of an ANN and show how they are trained using the so-called *backpropagation* algorithm.

5.1.1 ARCHITECTURE

An excellent introduction is given by Michael Nielsen in his freely available book "Neural networks and deep learning." The following section has been strongly inspired

by his presentation.

At the basis of each neural network lies the neuron. It transforms several inputs non-linearly into an output and we can use several neurons in parallel to create a *layer*. In turn, we several layers in series make up a network. The layers in the middle of the network are known as *hidden layers*, as shown in figure fig. 5.1.1
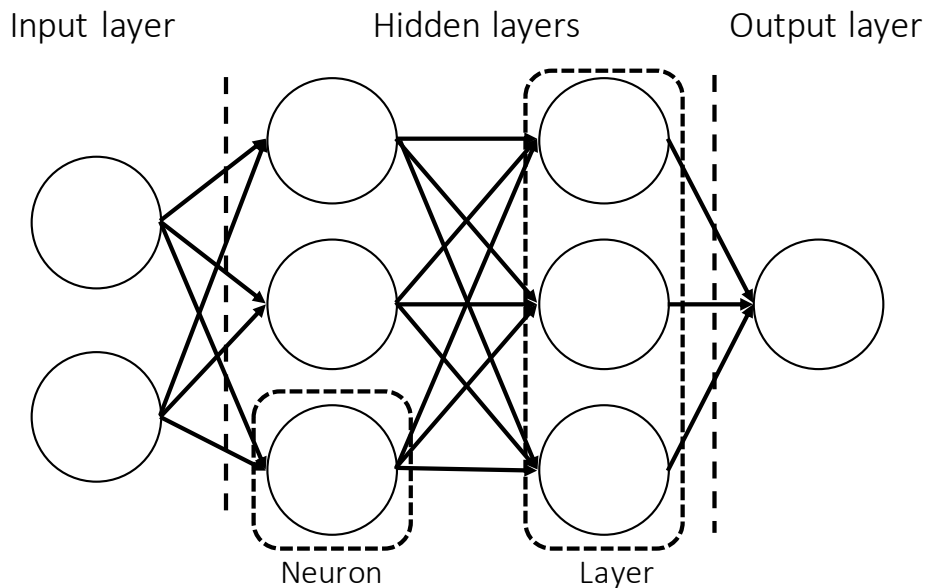
Input layer   Hidden layers   Output layer

Neuron   Layer

Figure 5.1.1: Schematic view of a neural network.

In the schematic shown in fig. 5.1.1, each neuron is connected to every neuron of the previous and next layer. This is known as a *fully connected* layer. Using only this type of layers, we've created a feed-forward network and it has been proven that a single hidden layer with enough neurons is a *universal function approximator*, i.e. a neural network can represent any continuous function using enough neurons.

As stated, a neuron takes several inputs and transforms them into an output. This is a two step process, where in the first step the neuron multiplies the input vector

$\mathbf{x}$ with a weight vector w and adds a bias b:

$$z = w\mathbf{x} + b \qquad (5.1)$$

z is called the weighted input and is transformed in the second step by the neuron *activation function* σ. This in turn gives the output of the neuron a, also known as the activation:

$$a = \sigma(z) = \sigma(w\mathbf{x} + b) \qquad (5.2)$$

The role of the activation function is to introduce non-linearity into the system. The classical and often used activation function is the *tanh*, as it is bounded between +1 and -1. Since we're working with multiple layers, it is useful to rewrite function eq. 5.2 in terms of the activation a^l of layer l:

$$a^l = \sigma(z^l) = \sigma(w^l a^{l-1} + b^l)$$

where w^l and b^l are respectively the weight matrix and bias of layer l.

5.1.2 TRAINING

In supervised learning the task of training a machine means adjusting the weights and biases until the neural network predictions match the desired outputs. We thus need some sort of metric to define this 'distance' between prediction and desired output. Training the network than means minimizing the metric with respect to the weights and biases of the network. This metric is known as the cost function $\mathcal{L}$ and the most used form is a mean squared error:

$$\mathcal{L} = \frac{1}{2n} \sum_i |y_i - a_i^L|^2 \qquad (5.3)$$

where n is the number of samples, y_i the desired output of sample i and a_i^L the activation of the last function - the prediction of the network. Minimizing this is not trivial, as the problem can have many local minima. A solution can be found however using gradient descent techniques.

Gradient descent techniques are based on the fact that given an initial position, the fastest way to reach the minimum from that position is by following the steepest gradient. Thus, given a function $f(\mathbf{x})$ to minimize w.r.t to $\mathbf{x}$, we guess an initial position x_n and iteratively change until it convergences:

$$\mathbf{x}_{n+1} = \mathbf{x}_n - \gamma \nabla f(\mathbf{x}_n)$$

where γ is known as the learning rate. If a global minimum exists, this technique will converge on it. More advanced versions of this technique exist which are able to deal with local minima as well, since convexity of the cost function is not at all guaranteed.

Making use of gradient descent requires knowledge of the derivatives of the cost function w.r.t to the variables to be optimized. In the case of neural networks, we thus need to know the derivative w.r.t to each weight and bias. A naive finite difference scheme would quickly grow computationally untractable for even shallow networks. A solution to this problem was found by Werbos in the form of the backpropagation algorithm. Despite many years of ongoing research, it is still the go-to algorithm for each neural network implementation.

Back propagation and automatic differentiation

As we wish to minimize the cost function w.r.t. to each weight w and bias b using gradient descent, we need to find the derivative of the cost function w.r.t to each. Our argument simplifies if we move away from vector notation and introduce w_{jk}^l, the weight of the j-th neuron in layer $l-1$ to neuron k in layer l and b_j^l, the bias of the neuron j in the l-th layer. We introduce the error of neuron j in layer l as:

$$\delta_j^l = \frac{\partial C}{\partial z_j^l}$$

We can rewrite this using the chain rule as:

$$\delta_j^l = \sum_k \frac{\partial C}{\partial a_{jk}^l} \frac{\partial a_{jk}^l}{\partial z_j^l}$$

However, the second term is always zero except when $j = k$, so the summation can be dropped. Remembering eq. 5.2, we note that $\partial a_{jk}^l / \partial z_j^l = \sigma'(z_j^l)$. For the last layer $l = L$, the first term turns into the derivative of the cost function, finally giving us:

$$\delta_j^L = |a_j^L - y_j|\sigma'(z_j^L) \tag{5.4}$$

Equation eq. 5.4 relates the error in the output layer to its inputs. This in turn is a function of all the previous inputs and errors and we thus need to find an expression relating the error in layer l with the error in an layer $l + 1$. Since we have an expression for the error in the last layer, we propagate the error going down the layers, hence the name *back*propagation. Again using the chain rule gives:

$$\delta_j^l = \sum_k \frac{\partial C}{\partial z_{jk}^{l+1}} \frac{\partial z_{jk}^{l+1}}{\partial z_j^l} = \sum_k \delta_k^{l+1} \frac{\partial z_{jk}^{l+1}}{\partial z_j^l}$$

Using equation eq. 5.1, we obtain after substitution:

$$\delta_j^l = \sum_k \delta_k^{l+1} w_{kj}^{l+1} \sigma'(z_j^l) \tag{5.5}$$

Using equations eq. 5.4 and eq. 5.5 , we can calculate the error in C due to each neuron. Finally, we need to relate the error in each error to $\partial C/\partial w_{jk}^l$ and $\partial C/\partial b_j^l$.

Making use yet again gives us the last two backpropagation relations:

$$\frac{\partial C}{\partial b_j^l}\frac{\partial b_j^l}{\partial z_j^l} = \frac{\partial C}{\partial b_j^l} = \delta_j^l \tag{5.6}$$

$$\sum_k \frac{\partial C}{\partial w_{jk}^l}\frac{\partial w_{jk}^l}{\partial z_j^l} = \delta_j^l \rightarrow \frac{\partial C}{\partial w_{jk}^l} = a_j^{l-1}\delta_j^l \tag{5.7}$$

Now that we now that all back propagation equations, we state the algorithm. It consists of four steps:

1. Complete a forward pass, i.e., calculate the expected outcomes with the current weights and biases.
2. Calculate the error using eq. 5.4 and do a backward pass to obtain the error in each neuron using eq. 5.5. This can be used to calculate the gradients using eq. 5.6 and eq. 5.7
3. Adjust the weights and biases using the choosen optimizer (e.g. gradient descent)
4. Return to step 1 until the optimization problem converges.

Mathematically, back propagation is a special case of a technique known as automatic differentiation. Automatic differentiation is a third type of differentiation, next to numeric and symbolic. It allows for machine precision calculation of derivatives by writing it as a chain of simple operations combined with the chain rule, similar to backpropagation. Note that:

$$\delta_j^o = \frac{\partial C}{\partial x_j}\frac{\partial x_j}{\partial z_j^o}$$

so that:

$$\frac{\partial C}{\partial x_j} = a_j^o \delta_j^o$$

Thus neural networks also give us access to high precision derivatives with regard to each coordinate.

5.2 Physics Informed Neural Networks

On the face of things, the goal of physics and neural networks are oppsite: whereas physics tries to build an understanding of things using models to make predictions, neural networks learn a *modelless* mapping to make predictions. Recent advancements however have merged the two approaches together in a concept known as Physics Informed Neural Networks (5, 4). In this approach, we encode physical laws into the network, so that the network respects the physics. This can be used to both numerically solve equations or fit a model to spatiotemporal data. Even more so, it should allow us to infer coefficient fields.

5.2.1 The concept

Consider a set of 1D+1 spatiotemporal data, consisting of some property $u(x, t)$ at coordinates (x, t). The neural network can be learned the underlying physics by minimizing the cost function:

$$\mathcal{L} = \frac{1}{2n} \sum_i |u_i - a_i^L|^2$$

The process of learning requires a lot of data and is prone to overfitting. Now assume that we know that $u(x, t)$ is governed by some process which is written as a partial differential equation:

$$\partial_t u = f(1, u, u_x, u_x x, u^2, \ldots)$$

where f is a function of u or its spatial derivatives. Rewriting it as:

$$g = 0 = -\partial_t u + f(1, u, u_x, u_x x, u^2, \ldots) \qquad (5.8)$$

we see that in order to satisfy the PDE, $g \to 0$. The idea of PINNs is to add this function g to the costfunction of the neural network:

$$\mathcal{L} = \frac{1}{2n} \sum_i |u_i - a_i^L|^2 + \lambda \sum_i |g_i|^2 = MSE + \lambda PI$$

where λ sets the effective strength of the two terms. Observe that the cost function is higher if the PDE is not satisfied. Minimizing the costfunction will thus mean minimizing g and hence satisfying the PDE. We effectively penalize solutions not satisfying the physics we put in equation eq. 5.8; the added term acts a 'physics-regularizer'. Concretely, the adding of physics contrains the solution space, preventing overfitting and making the neural network much more data efficient. The most useful feature however is that we don't need a vast set of training data to train the network, as we solve the problem *by* training the network.

We can also remove the mean squared error term from the cost function and add initial and boundary conditions, similar to the PI term. If we now train the network, it will learn the solution to the given PDE whilst respecting the given boundary and initial conditions. This alternative means of numerically solving a model doesn't need advanced meshing of the problem domain or carefully constructed (unstable) discretization schemes, as it requires the physics to be fullfilled at every point in the spatiotemporal domain. A useful analogy here is calculating the trajectory of a launched object. A classical numerical solver would take small steps in time, updating the position and speed of the object each step. A PINN however uses a completely different approach. Given the initial (random) state of the neural network, it calculates a first trajectory and keeps adjusting the weights of the network until the cost is minimized, i.e. until we obtain a solution

satisfying the included physics and initial and boundary conditions. A classical numerical approach tries once using a correct and methodical approach, whereas a PINN tries many times until the result satisfies its constraints.

We can also use this framework to fit models to spatiotemporal data by letting the coefficient of each term be a variable to be minimized as well. More concretely, where before the cost was a function of the weights and biases, $\mathcal{L} = f(w^l, b^l)$, we now let it be a function of the coefficients λ of the PDE as well: $\mathcal{L} = f(w^l, b^l, \lambda_1, \lambda_2, ...)$. This is shown for several PDEs such as the Burgers, Schrodinger or Navier-Stokes equation in the papers of M. Raissi(5, 4). In the case of the Navier-Stokes equation, it's shown that it's also possible to infer the pressure field, which appears as a separate term. This is achieved by adding another output neuron to the PINN (shown in figure fig. 5.2.1), so that it predicts both the pressure and the flow. In theory it should also be possible to infer spatially and temporally varying *coefficient* fields. We investigate this claim in the next section.
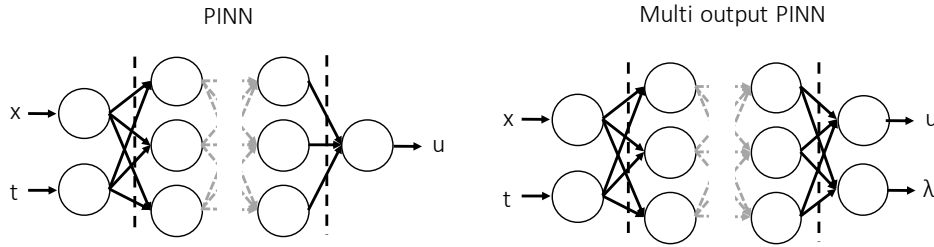

Figure 5.2.1: Left panel: a normal single output PINN. Right panel: a multi-output PINN. The network now also predicts the coefficients values at each data point.

5.2.2   PINNs in practice

We now wish to evaluate the use of PINNs to analyze the RUSH data. Using a diffusive process as a toy problem, we first show how PINNs are able to accurately determine the diffusion constant, even in the presence of noise. Next,

we prove that PINNs are indeed capable of inferring coefficient fields and finish by analyzing some parts of the RUSH data.

In our toy problem we have an initial concentration profile:

$$c(x, 0) = e^{-\frac{(x-0.5)^2}{0.02}}$$

diffusing in a 1D box according to:

$$\frac{\partial c(x, t)}{\partial t} = \nabla \cdot [D(x)\nabla c(x, t)]$$

on the spatial domain $[0, 1]$ with perfectly absorbing boundaries at the edges of the domain:

$$c(0, t) = c(1, t) = 0$$

If $D(x) = D$, this problem has an analytical solution through a Greens function. If the diffusion coefficient is spatially dependent though, we problem needs to be solved numerically. The code used to generate our data can be found in the appendix.

5.2.2.1 Constant diffusion coefficient

NOISELESS

Now consider the problem with a constant diffusion of $D_0 = 0.01$. We simulate the data on a domain $x : [0, 1]$ and $t : [0, 0.5]$ we use a spatial resolution of 0.01, giving the number of points 101 by 51, giving a total number of data points of 5151. Since the fitting is the training, we do not need to separate the data in a training and validation set. Figure ref shows the input data and the what the network predicts. After training, the network predicts (almost exactly) what we want it to and the average error is less than 1. Ofcourse, more interesting is the

inferred diffusion parameter. With a value of 0.10034, the error is roughly 0.3. This is very good, but ofcourse our data is without noise. Note however that even still is extremely good and that in their papers Raissi shows far more complex equations such as the complex Schrodinger one. Also note that the error is mostly located at areas with low signal. This is a consistent problem and must be taken into account. Powerful as they are, neural networks seem to struggle with this fig. **??** .
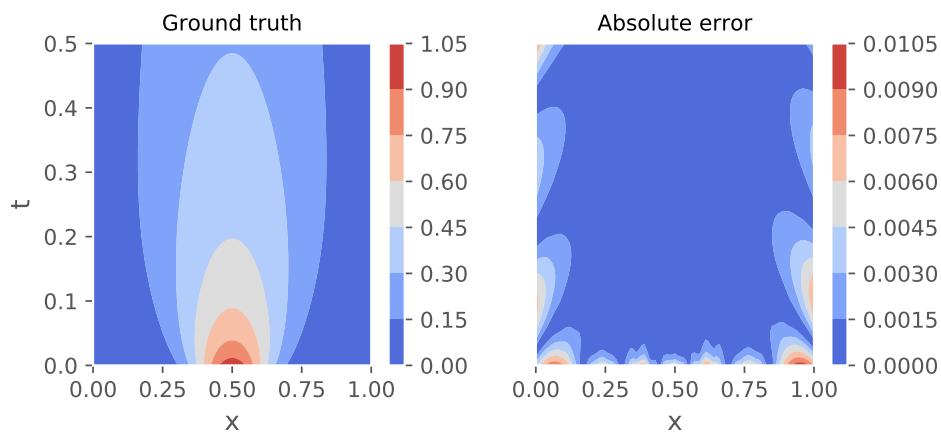

Figure 5.2.2: Left panel: something. Right panel: something else

Looks really nice.

Noisy

fig. **??** It becomes more interesting once we add noise. We take exactly the same problem, but now add 5% gaussian distributed white noise (e.g. $0.05std(c)$) and let the neural network do it's thing again. The network is now doing two things at once: it's *denoising* the data by stating that the underlying data is of a certain model while finding the optimal model parameters. Again figure **ref** shows our original data and the fit.

The data correctly infers the ground truth. The inferred diffusion coefficient is

0.10017, an error of 0.17. I just want to state that this is almost ridiculous. We have roughly 5000 points with 5 error and the network is able to infer the coefficent within 1. We also havent optimized the network in any way: it's the most basic full connected layers with tanh activation function and we just used enough layers and neurons. It's also a very general technique: it works for whatever PDE and data multidimensional data. We also fit the model directly to the data; circumventing the need to know boundary conditions, initial conditions etc… We can now proceed to more advanced setup.
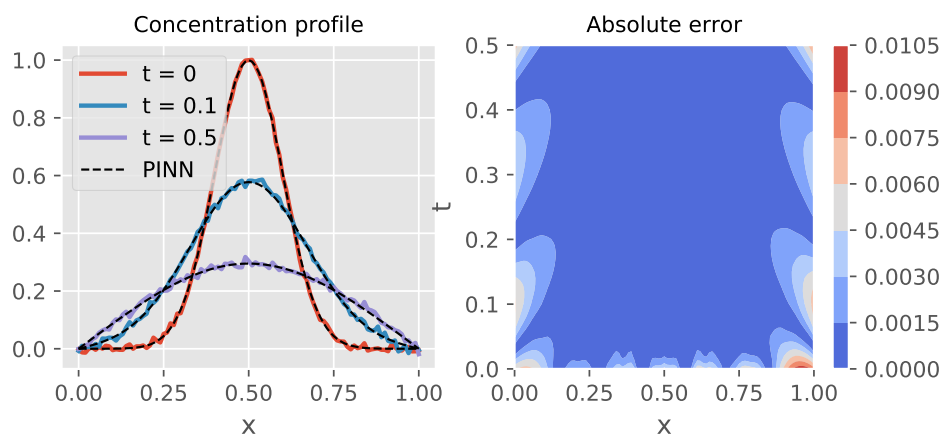

Figure 5.2.3: Left panel: something. Right panel: something else

5.2.2.2 VARYING D

As stated, it should be possible to infer varying coefficient fields. Instead of using a single output network, we implement of two output neural network; outputting both the coefficient and the concentration. Note that this is slightly different from what is done in this paper **ref**. They infer the pressure field, but this is a separate added term; its not multiplied by a spatially varying term.

Non-varying

We first demonstrate this using the same data as before: so although we allow a spatially varying field, the underlying data only has a single diffusion coefficient. The coefficient is then learned through training the network and 'corrected' by PI-loss function. Figure **ref** shows our results.

test reference[4]

and another one

Varying

5.2.2.3 Real cell

5.3 Conclusion

5.3.1 Weak points and how to improve

6
Conclusion

Appendix 1: Some extra stuff

Add appendix 1 here. Vivamus hendrerit rhoncus interdum. Sed ullamcorper et augue at porta. Suspendisse facilisis imperdiet urna, eu pellentesque purus suscipit in. Integer dignissim mattis ex aliquam blandit. Curabitur lobortis quam varius turpis ultrices egestas.

References

1. Karpatne, A., Watkins, W., Read, J. & Kumar, V. Physics-guided Neural Networks (PGNN): An Application in Lake Temperature Modeling. *arXiv:1710.11431 [physics, stat]* (2017).

2. Sharma, R., Farimani, A. B., Gomes, J., Eastman, P. & Pande, V. Weakly-Supervised Deep Learning of Heat Transport via Physics Informed Loss. *arXiv:1807.11374 [cs, stat]* (2018).

3. Pun, G. P. P., Batra, R., Ramprasad, R. & Mishin, Y. Physically-informed artificial neural networks for atomistic modeling of materials. *arXiv:1808.01696 [cond-mat]* (2018).

4. Raissi, M., Perdikaris, P. & Karniadakis, G. E. Physics Informed Deep Learning (Part II): Data-driven Discovery of Nonlinear Partial Differential Equations. *arXiv:1711.10566 [cs, math, stat]* (2017).

5. Raissi, M., Perdikaris, P. & Karniadakis, G. E. Physics Informed Deep Learning (Part I): Data-driven Solutions of Nonlinear Partial Differential Equations. *arXiv:1711.10561 [cs, math, stat]* (2017).